Atmospheric ammonia measurements and implications for particulate matter formation in Houston, TX

Longwen Gong[†], *Rafal Lewicki*[‡], *Robert J. Griffin*[†], *Frank K. Tittel*[‡], *Chantelle R. Lonsdale*[§], *Robin G. Stevens*[§], *Jeffrey R. Pierce*[§], *Quentin G. J. Malloy*[†⊥], *Severin A. Travis*[†#], *Loliya M. Bobmanuel*[†▽], *Barry L. Lefer*[‖], *and James H. Flynn*[‖]

[†]Department of Civil and Environmental Engineering, Rice University, Houston, TX, USA

[‡]Department of Electrical and Computer Engineering, Rice University, Houston, TX, USA

[§]Department of Atmospheric Science, Dalhousie University, Halifax, Nova Scotia, Canada

[‖]Department of Earth and Atmospheric Sciences, University of Houston, Houston, TX, USA

[⊥]Now at RTI International, Research Triangle Park, NC, USA

[#]Now at Environmental Resources Management, Houston, TX, USA

[▽]Now at USA Environment, L.P., Houston, TX, USA

Corresponding Author

Phone: (713) 348-2093, email: rob.griffin@rice.edu.

Abstract

Simultaneous measurements of atmospheric NH_3, HNO_3, soluble gas-phase chloride, and aerosol species were made in Houston, TX, from August 5, 2010 to August 9, 2010. Gaseous NH_3 was measured using a 10.4-μm external cavity quantum cascade laser-based sensor employing conventional photo-acoustic spectroscopy, while gaseous HNO_3 and HCl were sampled using a mist chamber-ion chromatograph (IC) system. Particle chemical composition was determined using a particle-into-liquid-sampler-IC system. There was a large amount of variability in the mixing ratios of NH_3 (3.0 ± 2.5 ppb), HNO_3 (287.4 ± 291.6 ppt), and HCl (221.3 ± 260.7 ppt). Elevated NH_3 levels occurred around mid-day when NH_4^+ (0.5 ± 1.0 μg/m^3) and SO_4^{2-} (4.5 ± 4.3 μg/m^3) also increased considerably, indicating that NH_3 had a strong impact on aerosol particle mass. By contrast, the formation of NH_4NO_3 and NH_4Cl was not observed during the campaign. Power plant plumes were found to be potential contributors to the enhancements in NH_3 under favorable meteorological conditions. Increased particle number concentrations were predicted by the SAM-TOMAS model downwind of a large coal-fired power plant when NH_3 emissions based on these measurements were included. This study shows that NH_3 mixing ratios in the polluted Houston atmosphere occasionally exceeded previous modeling predictions, suggesting the influence of both local and regional sources while also highlighting the potential importance of NH_3 with respect to particle number concentration.

Key words: ammonia, particulate matter, gas-particle partitioning, aerosol nucleation.

Introduction

Ammonia (NH_3) is widely present in the atmosphere due to many anthropogenic and natural sources (1), usually at trace concentration levels ranging from parts per trillion (ppt) to parts per billion (ppb). However, agriculture (e.g., fertilizer application and animal husbandry) (2, 3) and industrial and motor vehicle (e.g., chemical production and traffic emission) (4, 5) activities contribute to significant increases in local and/or regional NH_3 levels. In addition, National Emissions Inventory air pollutant emissions trends data prepared by the United States Environmental Protection Agency (U.S. EPA) indicate that annual NH_3 emissions from the source category of electric utilities have risen continuously since 2005. Gaseous NH_3 can increase particulate matter (PM) mass concentrations through the formation of ammonium salts such as ammonium sulfate ($(NH_4)_2SO_4$), ammonium nitrate (NH_4NO_3), and ammonium chloride (NH_4Cl) via chemical reactions with sulfuric, nitric, and hydrochloric acids, respectively. Experiments also reveal that NH_3 plays a vital role in aerosol nucleation events (6-8).

The resultant PM affects the Earth's radiation budget through direct and/or indirect effects and modifies the properties of clouds by serving as cloud condensation and/or ice nuclei (9). Epidemiological studies also have demonstrated a strong correlation between human exposure to PM and increased rates of respiratory and cardiovascular illness and other adverse human health effects (10, 11). Despite these implications for ammonia's negative impacts on air quality, NH_3 currently is not regulated under the National Ambient Air Quality Standards by the U.S. EPA. As a result, there are

substantial uncertainties in spatial and temporal variations of NH_3 due to the lack of ground-based observations.

Conventional NH_3 studies primarily have focused on the measurements near source areas (e.g., farms) (12, 13) using passive samplers (e.g., annular diffusion denuders) with off-line analysis (e.g., ion chromatography (IC)) (14, 15). Newly developed NH_3 instruments using laser spectroscopy and chemical ionization mass spectrometry have improved time resolution and detection limits and minimized human-induced errors (16, 17). Meanwhile, relatively little previous work has investigated the effect of gas-particle partitioning of NH_3 and the interaction between NH_3 and acidic gaseous and particulate species due to a paucity of simultaneous datasets. In addition, information about NH_3 levels for the industrial and urban area of Greater Houston is still scarce. Nowak et al. (18) conducted a 14-day aircraft measurement campaign including atmospheric NH_3 along the Houston Ship Channel (HSC) area during the second Texas Air Quality Study (TexAQS II). Gong et al. (19) characterized the seasonal and diurnal patterns of gaseous NH_3 levels in Houston. According to a photochemical model, the estimated NH_3 mixing ratios for the Houston area are in the range of 1 to 15 ppb (20). In order to examine the effects of NH_3 on air quality in Houston, measurements of gas-phase NH_3, nitric acid (HNO_3), soluble chloride (assumed to be hydrochloric acid (HCl)), and aerosol species were performed during the summer of 2010 by simultaneous on-line gas- and particle-phase instrumentation.

Materials and Methods

In this study, the simultaneous measurements of trace gases and particle chemical composition were carried out from August 5, 2010 to August 9, 2010. All instruments were deployed in a trailer atop an 18-story (~65 m above ground level) building (North Moody Tower) located on the University of Houston (UH) main campus, which is influenced by many local and regional emission sources such as highways, airports, and industrial facilities. Detailed information about this sampling site can be found in Lefer and Rappenglück (21). Meteorological parameters (e.g., temperature and relative humidity) as well as mixing ratios of some important air pollutants (e.g., carbon monoxide (CO)) are measured regularly by the UH research group at this location (22, 23). All data were averaged into 1-hr intervals for temporal consistency.

Gaseous species measurements

Gas-phase NH_3 was measured using a 10.4-μm external cavity quantum cascade laser-based sensor employing conventional photo-acoustic spectroscopy as described in Gong et al. (19). This state-of-the-art optical technique achieves a sub-ppb detection limit with a response time of seconds and an accuracy of ~6%. Gas-phase HNO_3 and HCl were measured using a mist chamber together with IC (Dionex, Model CD20-1), where the minimum detection limits of ppt levels were reached for a temporal resolution of 10 minutes with an uncertainty of ±10% (23, 24).

Aerosol species measurements

Particle chemical composition was measured using a particle-into-liquid-sampler (PILS) (BMI, Model 4002) coupled directly to two IC systems (Dionex, Model 1600) (25, 26). Mass concentrations ($\mu g/m^3$) of water soluble inorganic components including ammonium (NH_4^+), sodium (Na^+), potassium (K^+), calcium (Ca^{2+}), magnesium (Mg^{2+}), sulfate (SO_4^{2-}), nitrate (NO_3^-), nitrite (NO_2^-) and chloride (Cl^-) in fine particle aerosols ($D_p < 1$ μm) were determined at 16-min intervals.

Results and Discussion

Effect of NH_3 on Particle Mass Concentrations

Figure 1 presents a time series of hourly-averaged mixing ratios (± one standard deviation) of gaseous NH_3 (3.0 ± 2.5 ppb), HNO_3 (287.4 ± 291.6 ppt), HCl (221.3 ± 260.7 ppt) and CO (109.8 ± 22.4 ppb) and concentrations of particulate NH_4^+ (0.5 ± 1.0 $\mu g/m^3$), SO_4^{2-} (4.5 ± 4.3 $\mu g/m^3$), NO_3^- (0.3 ± 0.2 $\mu g/m^3$) and Cl^- (0.2 ± 0.1 $\mu g/m^3$) along with meteorological parameters. The NH_3 mixing ratios are a subset of the data considered by Gong et al. (19). NH_3 levels were elevated around mid-day, when NH_4^+ and SO_4^{2-} also dramatically increased compared to other time periods of the measurements. This suggests that NH_3 played an important role in PM formation and that the gas-particle conversion was highly efficient when NH_3 was available, though SO_4^{2-} goes to the aerosol phase regardless of NH_3 level. However, NO_3^- and Cl^- concentrations did not change significantly throughout the campaign.

During these peaks, the wind mainly blew from the southwest in the direction of the second largest coal-fired power plant (W. A. Parish) in the U.S. (also verified by Hybrid Single-Particle Lagrangian Integrated Trajectory modeling (27)). The average wind speed was about 10 miles per hour when these mid-day spikes occurred, leading to an inference that the electricity generating station, which is approximately 23 miles (37 km) away from the sampling site, may be a source of NH_3 in Houston during this period. The selective catalytic reduction (SCR) technique was installed to control nitrogen oxides (NO_x) emissions from Parish after 2000 (28). Interestingly, no NH_3 spikes in Parish plumes were reported by Nowak et al. (18). Auxiliary data collected atop the Moody Tower were used to assist in NH_3 source identification. For instance, primary pollutants such as CO emitted from automobile tailpipes are usually used as indicators of vehicular emissions. Since the introduction of three-way catalytic converters, motor vehicles have contributed to elevated NH_3 levels in urban areas (29, 30) when NO_x is over-reduced inside the converters (31, 32). Nevertheless, no enhancements in CO were coincident with enhanced NH_3 around mid-day, indicating that motor vehicles are less likely to cause elevated NH_3 in Houston during this period.

During the five days of measurements, there were no concurrent decreases in HNO_3 and HCl nor increases in NO_3^- and Cl^- when NH_3 levels were elevated around mid-day, indicating that NH_4NO_3 and NH_4Cl were not formed. This speculation is verified by the very low saturation ratios (<< 1) illustrated in Figure 2. The saturation ratio is the partial pressure product ($P_{NH_3}P_{HNO_3}$ or $P_{NH_3}P_{HCl}$) divided by the dissociation

constant ($K_{NH_4NO_3}$ or K_{NH_4Cl}) that can be calculated using empirical equations (33, 34) based on the reversible formation of NH_4NO_3 and NH_4Cl (eqs 1 and 2).

$$NH_3(g) + HNO_3(g) \leftrightarrow NH_4NO_3(s\ or\ aq) \quad (1)$$

$$NH_3(g) + HCl(g) \leftrightarrow NH_4Cl(s\ or\ aq) \quad (2)$$

Particulate NH_4NO_3 and NH_4Cl condense when the saturation ratio is larger than one, and they evaporate when the saturation ratio is smaller than one. This is in contrast to the study of Nowak et al. (18) during TexAQS II who observed NH_4NO_3 formation in HSC plumes with elevated NH_3 levels ranging from 5 to 80 ppb, likely due to the shift in the thermodynamic equilibrium towards the aerosol phase caused by very high NH_3 mixing ratios. Because the time scales to achieve thermodynamic equilibrium for NH_4NO_3 and NH_4Cl usually are on the order of minutes under ambient conditions (35, 36), the time since emission likely can be eliminated as the reason for the lack of NH_4NO_3 and NH_4Cl formation in the present work. However, relatively high temperatures (30.1 ± 2.3 ^oC) likely do inhibit the formation of NH_4NO_3 and NH_4Cl because volatilization increases with temperature; by contrast, sulfate is considered essentially non-volatile (37). The Aerosol Inorganics Model also was employed, and it yielded similar results for the calculation of thermodynamic equilibrium/gas-particle partitioning using measurement data from this study (38).

A regression between measured molar concentrations of cations and anions yields a strongly linear relationship (Figure 3, R^2 = 0.96; $p < 0.0001$; slope = 1.53), suggesting that SO_4^{2-}, NO_3^- and Cl^- (The rest of the anions were minor.) were largely associated with NH_4^+ (The rest of the cations other than H^+ were minor.) and that ambient

aerosols were likely acidic as a result of incomplete neutralization. However, the average value of the molar concentration ratio of gaseous NH_3 to total NH_3 (the sum of NH_3 and NH_4^+), also known as the gas fraction ($\sigma = 0.86 \pm 0.17$), shows that NH_3 remained predominantly in the gas phase rather than the aerosol phase, as shown in Figure 4, although sampled aerosols were ammonium-poor.

It is unlikely that aerosols are high in acid content when gaseous NH_3 is prevalent in the atmosphere. There may be cations present in aerosols not measured with the PILS-IC. One, though not the only possible, hypothesis is that amines contribute to the cationic composition of PM. Amines widely exist in the atmosphere from a variety of sources, and they are subject to physical and chemical processes such as gas-particle partitioning (39, 40). It has been reported that aminium can displace NH_4^+ in ammonium salts (41, 42). In addition, the availability of amines enhances sulfuric acid-water (H_2SO_4-H_2O) nucleation (43, 44), which may partially account for relatively high SO_4^{2-} levels (up to 33.7 $\mu g/m^3$) observed during the measurements. If we assume that ambient aerosols are neutral and attribute all missing cations to aminium, the estimated required mixing ratio of gaseous amines is approximately 55 ppb following the example in Ge et al. (40). While this is a very large value, observed atmospheric amine mixing ratios range from ppt to hundreds of ppb levels; even parts per million (ppm) levels were found in power plant regions (45). Some existing plants in the U.S. use amine-based solvent to capture post-combustion carbon dioxide (46). However, to our knowledge, Parish currently uses only NH_3 tank farms instead of amine technology. Given the strong linear relationship between

measured anions and cations, the aminium concentrations would be correlated strongly with NH_4^+ if present.

It is also noted that the mean gas fractions for HNO_3 ($\sigma = 0.71 \pm 0.14$) and HCl ($\sigma = 0.72 \pm 0.24$) were larger than 0.5, as shown in Figure 4, indicating they existed mainly in the gas phase. This observation may be attributed to the warm conditions during the measurements, which favor volatilization of NH_4NO_3 and NH_4Cl. Figure 5 displays the molar concentration ratio of NH_3 to the sum of HNO_3 and HCl (11.3 ± 9.5) over the entire course of sampling, indicating that NH_3 was much more abundant than HNO_3 and HCl.

Effect of NH_3 on Particle Number Concentrations

Aerosol nucleation and growth in coal-fired power plant plumes can greatly contribute to particle number concentrations near source regions. Stevens et al. (47) incorporated the TOMAS aerosol microphysics module (48, 49) into the SAM Large-Eddy Simulation/Cloud Resolving model (50) (SAM-TOMAS) and simulated aerosol nucleation and growth in the Parish power-plant plume. In the present work we also used this model to investigate how NH_3 emissions from power plants may affect the nucleation and growth of particles in the plume. The model simulates the aerosol size distribution using 15 size bins segregated by dry mass per particle covering a size range from 3 nm to 10 μm and microphysical processes including coagulation, H_2SO_4 condensation, and nucleation (47). Modeled H_2SO_4 vapor formation depends on SO_2 and OH concentrations, and the OH concentrations in turn

depend on the amount of sunlight and the NO_x concentrations.

NH_3 is considered to be a potentially important participant in aerosol nucleation and formation. In order to evaluate the effects of NH_3 on particle number concentration along the trajectory of power plant plumes, we hypothesize that elevated NH_3 levels originated from NH_3 slips at Parish, and we add NH_3 emissions from the plant to the SAM-TOMAS simulations. Two ternary (H_2SO_4-H_2O-NH_3) nucleation schemes, Merikanto et al. (51) and Napari et al. (52) (which is scaled by a factor of 10^{-5} to better agree with observations (53)), are tested in SAM-TOMAS. Figure 6 shows twelve simulations from SAM-TOMAS under various environmental conditions. It shows the number of new particles in the plume normalized by the SO_2 emitted as a function of the distance downwind from the plant. Both schemes were run with 900 ppt and 0 ppt NH_3 background mixing ratios. In addition, three different NH_3 emission scenarios (high: 0.012 kg/s; medium: 0.007 kg/s; low: 0.0012 kg/s) were employed and tested based on the calculated range of NH_3 emission factors (82,500 to 825,000 lb/yr) from Parish based on vendor-estimated slip values (1 to 10 ppm) (54). In all simulations, the number of new particles reaches a maximum near 10 km downwind; beyond this point, concentrations decrease because coagulation rates exceed nucleation rates. It can be seen that NH_3 emissions are very important for new particle formation, especially in the simulations in which background NH_3 mixing ratios are low (i.e., the green and red lines show a large variation in nucleation between simulations with different NH_3 emission rates). When background NH_3 mixing ratios were larger, the simulated effect of NH_3 emissions on nucleation was

more saturated and the predicted differences between NH_3 emission scenarios were smaller. Specifically, the fractional increases in particle concentrations between the low and high NH_3 emission simulations at 50 km downwind were 1.1 for Merikanto's nucleation scheme with 900 ppt NH_3 background mixing ratio, 2.0 for Merikanto's nucleation scheme with 0 ppt NH_3 background mixing ratio, 1.2 for Napari's nucleation scheme with 900 ppt NH_3 background mixing ratio, and 2.5 for Napari's nucleation scheme with 0 ppt NH_3 background mixing ratio, respectively. Larger NH_3 emissions accelerate aerosol nucleation in the simulations, as the system exhibits a high sensitivity to the amount of NH_3 slip, which emphasizes the significance of future NH_3 measurements in areas near power plants that utilize SCR. In addition, although Houston is currently in compliance with the mass-based $PM_{2.5}$ standards, efforts to characterize particle number concentration and size distribution synchronously with measurements of gaseous and particulate species are needed to better understand NH_3 impacts on both particle mass and number concentrations.

Acknowledgment

This study was supported by the Mid-InfraRed Technologies for Health and the Environment (MIRTHE) Center and National Science Foundation (NSF) under grant No. EEC-0540832. Chantelle Lonsdale, Robin Stevens and Jeffrey Pierce were funded by the Electric Power Research Institute (EPRI). Robin Stevens is supported by an NSERC PGS-D graduate fellowship. The authors gratefully acknowledge the NOAA Air Resources Laboratory (ARL) for the provision of the HYSPLIT transport

and dispersion model and/or READY website (http://www.arl.noaa.gov/ready.php) used in this publication. The authors also would like to thank Melanie Calzada and Kabindra Shakya for their help in data collection and preparation.

References

1. Clarisse, L.; Clerbaux, C.; Dentener, F.; Hurtmans, D.; Coheur, P.-F. Global ammonia distribution derived from infrared satellite observations. *Nat. Geosci.* **2009**, *2*, 479–483, doi:10.1038/ngeo551.
2. Mount, G. H.; Rumburg, B.; Havig, J.; Lamb, B.; Westberg, H.; Yonge, D.; Johnson, K.; Kincaid, R. Measurement of atmospheric ammonia at a dairy using differential optical absorption spectroscopy in the mid-ultraviolet. *Atmos. Environ.* **2002**, *36*, 1799–1810.
3. Rumburg, B.; Mount, G. H.; Filipy, J.; Lamb, B.; Westberg, H.; Yonge, D.; Kincaid, R.; Johnson, K. Measurement and modeling of atmospheric flux of ammonia from dairy milking cow housing. *Atmos. Environ.* **2008**, *42*, 3364–3379.
4. Hsieh, L. T.; Chen, T. C. Characteristics of ambient ammonia levels measured in three different industrial parks in southern Taiwan. *Aerosol Air Qual. Res.* **2010**, *10*, 596–608.
5. Kean, A. J.; Harley, R. A. On-road measurement of ammonia and other motor vehicle exhaust emissions. *Environ. Sci. Technol.* **2000**, *34*, 3535–3539.
6. Kulmala, M.; Korhonen, P.; Napari, I.; Karlsson, A.; Berresheim, H.; O'Dowd, C. D. Aerosol formation during PARFORCE: Ternary nucleation of H_2SO_4, NH_3, and H_2O. *J. Geophys. Res.* **2002**, *107(D19)*, 8111, doi:10.1029/2001JD000900.
7. McMurry, P. H.; Fink, M.; Sakurai, H.; Stolzenburg, M. R.; Mauldin III, R. L.; Smith, J.; Eisele, F.; Moore, K.; Sjostedt, S.; Tanner, D.; Huey, L. G.; Nowak, J. B.; Edgerton, E.; Voisin, D. A criterion for new particle formation in the sulfur-rich Atlanta atmosphere. *J. Geophys. Res.* **2005**, *110*, D22S02, doi:10.1029/2005JD005901.
8. Kirkby, J.; Curtius, J.; Almeida, J.; Dunne, E.; Duplissy, J.; Ehrhart, S.; Franchin, A.; Gagné, S.; Ickes, L.; Kürten, A.; Kupc, A.; Metzger, A.; Riccobono, F.; Rondo, L.; Schobesberger, S.; Tsagkogeorgas, G.; Wimmer, D.; Amorim, A.; Bianchi, F.; Breitenlechner, M.; David, A.; Dommen, J.; Downard, A.; Ehn, M.; Flagan, R. C.; Haider, S.; Hansel, A.; Hauser, D.; Jud, W.; Junninen, H.; Kreissl, F.; Kvashin, A.; Laaksonen, A.; Lehtipalo, K.; Lima, J.; Lovejoy, E. R.; Makhmutov, V.; Mathot, S.; Mikkilä, J.; Minginette, P.; Mogo, S.; Nieminen, T.; Onnela, A.; Pereira, P.; Petäjä, T.; Schnitzhofer, R.; Seinfeld, J. H.; Sipilä, M.; Stozhkov, Y.; Stratmann, F.; Tomé, A.; Vanhanen, J.; Viisanen, Y.; Vrtala, A.; Wagner, P. E.; Walther, H.; Weingartner, E.; Wex, H.; Winkler, P. M.; Carslaw, K. S.; Worsnop, D. R.; Baltensperger, U.;

Kulmala, M. Role of sulphuric acid, ammonia and galactic cosmic rays in atmospheric aerosol nucleation. *Nature.* **2011**, *476*, 429-433.

9. *Atmospheric aerosol properties and climate impacts.* U.S. Climate Change Science Program. Synthesis and Assessment Product 2.3, **2009**.
10. Pope, C. A.; Burnett, R. T.; Thun, M. J.; Calle, E. E.; Krewski, D.; Ito, K.; Thurston, G. D. Lung cancer, cardiopulmonary mortality, and long-term exposure to fine particulate air pollution. *J. Am. Med. Assoc.* **2002**, *287*, 1132–1141.
11. Pope, C. A.; Dockery, D. W. Health effects of the fine particulate air pollution: lines that connect. *J. Air & Waste Manage. Assoc.* **2006**, *56*, 709–774.
12. Ferm, M.; Marcinkowski, T.; Kieronczyk, M.; Pietrzak, S. Measurements of ammonia emissions from manure storing and spreading stages in Polish commercial farms. *Atmos. Environ.* **2005**, *39*, 7106–7113.
13. Robarge, W. P.; Walker, J. T.; McCulloch, R. B.; Murray, G. Atmospheric concentrations of ammonia and ammonium at an agricultural site in the southeast United States. *Atmos. Environ.* **2002**, *36*, 1661-1674.
14. Wilson, S. M.; Serre, M. L. Use of passive samplers to measure atmospheric ammonia levels in a high-density industrial hog farm area of eastern North Carolina. *Atmos. Environ.* **2007**, *28*, 6074–6086.
15. Baek, B. H.; Aneja, V. P. Measurement and analysis of the relationship between ammonia, acid gases, and fine particles in eastern North Carolina. *J. Air & Waste Manage. Assoc.* **2004**, *54*, 623-633.
16. Nowak, J. B.; Neuman, J. A.; Kozai, K.; Huey, L. G.; Tanner, D. J.; Holloway, J. S.; Ryerson, T. B.; Frost, G. J.; McKeen, S. A.; Fehsenfeld, F. C. A chemical ionization mass spectrometry technique for airborne measurements of ammonia. *J. Geophys. Res.* **2007**, *112*, D10S02, doi:10.1029/2006JD007589.
17. Pogány, A.; Mohácsi, Á.; Jones, S. K.; Nemitz, E.; Varga, A.; Bozóki, Z.; Galbács, Z.; Weidinger, T.; Horváth, L.; Szabó, G. Evaluation of a diode laser based photoacoustic instrument combined with preconcentration sampling for measuring surface–atmosphere exchange of ammonia with the aerodynamic gradient method. *Atmos. Environ.* **2010**, *44*, 1490–1496.
18. Nowak, J. B.; Neuman, J. A.; Bahreini, R.; Brock, C. A.; Middlebrook, A. M.; Wollny, A. G.; Holloway, J. S.; Peischl, J.; Ryerson, T. B.; Fehsenfeld, F. C. Airborne observations of ammonia and ammonium nitrate formation over Houston, TX. *J. Geophys. Res.* **2010**, *115*, D22304, doi:10.1029/2010JD014195.
19. Gong, L.; Lewicki, R.; Griffin, R. J.; Flynn, J. H.; Lefer, B. L.; Tittel, F. K. Atmospheric ammonia measurements in Houston, TX using an external-cavity quantum cascade laser-based sensor. *Atmos. Chem. Phys.* **2011**, *11*, 9721-9733.
20. Pavlovic, R. T.; Nopmongcol, U.; Kimura, Y.; Allen, D. T. Ammonia emissions, concentrations and implications for particulate matter formation in Houston, TX. *Atmos. Environ.* **2006**, *40*, 538–551.
21. Lefer, B.; Rappenglück, B. The TexAQS-II radical and aerosol measurement project (TRAMP). *Atmos. Environ.* **2010**, *44*, 3997–4004.

22. Lefer, B.; Rappenglück, B.; Flynn, J.; Haman, C. Photochemical and meteorological relationships during the Texas-II Radical and Aerosol Measurement Project (TRAMP). *Atmos. Environ.* **2010**, *44*, 4005–4013.
23. Luke, W. T.; Kelley, P.; Lefer, B.; Flynn, J.; Rappenglück, B.; Leuchner, M.; Dibb, J. E.; Ziemba, L. D.; Anderson, C. H.; Buhr, M. Measurements of primary trace gases and NO_Y composition in Houston, Texas. *Atmos. Environ.* **2010**, *44*, 4068–4080.
24. Dibb, J. E.; Scheuer, E.; Whitlow, S. I.; Vozella, M. Ship-based nitric acid measurements in the Gulf of Maine during New England Air Quality Study 2002. *J. Geophys. Res.* **2004**, *109*, D20303, doi:10.1029/2004JD004843.
25. Lee, Y.-N.; Weber, B.; Ma, Y.; Orsini, D.; Maxwell-Meier, K.; Blake, D.; Meinardi, S.; Sachse, G.; Harward, C.; Chen, T.-Y.; Thornton, D.; Tu, F.-H.; Bandy, A. Airborne measurement of inorganic ionic components of fine aerosol particles using the particle-into-liquid sampler coupled to ion chromatography technique during ACE-Asia and TRACE-P. *J. Geophys. Res.* **2003**, *108(D23)*, 8646, doi:10.1029/2002JD003265.
26. Orsini, D. A.; Ma, Y.; Sullivan, A.; Sierau, B.; Baumann, K.; Weber, R. J. Refinements to the particle-into-liquid sampler (PILS) for ground and airborne measurements of water soluble aerosol composition. *Atmos. Environ.* **2003**, *37*, 1243-1259.
27. Draxler, R. R.; Rolph, G. D. HYSPLIT (HYbrid Single-Particle Lagrangian Integrated Trajectory) Model access via NOAA ARL READY Website (http://ready.arl.noaa.gov/HYSPLIT.php). NOAA Air Resources Laboratory, Silver Spring, MD, **2012**.
28. Peischl, J.; Ryerson, T. B.; Holloway, J. S.; Parrish, D. D.; Trainer, M.; Frost, G. J.; Aikin, K. C.; Brown, S. S.; Dubé, W. P.; Stark, H.; Fehsenfeld, F. C. A top-down analysis of emissions from selected Texas power plants during Tex-AQS 2000 and 2006. *J. Geophys. Res.* **2010**, *115*, D16303, doi:10.1029/2009JD013527.
29. Perrino, C.; Catrambone, M.; Di Menno Di Bucchianico, A.; Allegrini, I. Gaseous ammonia in the urban area of Rome, Italy and its relationship with traffic emissions. *Atmos. Environ.* **2002**, *36*, 5385–5394
30. Kean, A. J.; Littlejohn, D.; Ban-Weiss, G. A.; Harley, R. A.; Kirchstetter, T. W.; Lunden, M. M. Trends in on-road vehicle emissions of ammonia. *Atmos. Environ.* **2009**, *43*, 1565–1570.
31. Heck, R. M.; Farrauto, R. J. Automobile exhaust catalysts. *Appl. Catal. A: General*. **2001** *221*, 443–457.
32. Heeb, N. V.; Forss, A.; Brühlmann, S.; Lüscher, R.; Saxer, C. J.; Hug, P. Three-way catalyst-induced formation of ammonia– velocity- and acceleration-dependent emission factors. *Atmos. Environ.* **2006**, *40*, 5986–5997.
33. Seinfeld, J. H.; Pandis, S. N. *Atmospheric Chemistry and Physics: From Air Pollution to Climate Change*; John Wiley: New York, **2006**.
34. Pio, C. A.; Harrison, R. M. The equilibrium of ammonium chloride aerosol with gaseous hydrochloric acid and ammonia under tropospheric conditions. *Atmos. Environ.* **1987**, *21*, 1243-1246.

35. Wexler, A. S.; Seinfeld, J. H. Analysis of aerosol ammonium nitrate: Departures from equilibrium during SCAQS. *Atmos. Environ.* **1992**, *26*, 579-591.
36. Meng, Z.; Seinfeld, J. H. Time scales to achieve atmospheric gas-aerosol equilibrium for volatile species. *Atmos. Environ.* **1996**, *30*, 2889-2900.
37. Bassett, M. E.; Seinfeld, J. H. Atmospheric equilibrium model of sulfate and nitrate aerosols – II. Particle size analysis. *Atmos. Environ.* **1984**, *18*, 1163-1170.
38. Wexler, A. S.; Clegg, S. L. Atmospheric aerosol models for systems including the ions H^+, NH_4^+, Na^+, SO_4^{2-}, NO_3^-, Cl^-, Br^-, and H_2O. *J. Geophys. Res.* **2002**, *107(D14)*, 4207, doi:10.1029/2001JD000451.
39. Ge, X.; Wexler, A. S.; Clegg, S. L. Atmospheric amines – Part I. A review. *Atmos. Environ.* **2011**, *45*, 524-546.
40. Ge, X.; Wexler, A. S.; Clegg, S. L. Atmospheric amines – Part II. Thermodynamic properties and gas/particle partitioning. *Atmos. Environ.* **2011**, *45*, 561-577.
41. Smith, J. N.; Barsanti, K. C.; Friedli, H. R.; Ehn, M.; Kulmala, M.; Collins, D. R.; Scheckman, J. H.; Williams, B. J.; McMurry, P. H. Observations of aminium salts in atmospheric nanoparticles and possible climatic implications. *Proc. Natl. Acad. Sci.* **2010**, *107* (15), 6634-9.
42. Bzdek, B. R.; Ridge, D. P.; Johnston, M. V. Amine exchange into ammonium bisulfate and ammonium nitrate nuclei. *Atmos. Chem. Phys.* **2010**, *10*, 3495-3503.
43. Kurtén, T.; Loukonen, V.; Vehkamäki, H.; Kulmala, M. Amines are likely to enhance neutral and ion-induced sulfuric acid-water nucleation in the atmosphere more effectively than ammonia. *Atmos. Chem. Phys.* **2008**, *8*, 4095-4103.
44. Loukonen, V.; Kurtén, T.; Ortega, I. K.; Vehkamäki, H.; Pádua, A. A. H.; Sellegri, K.; Kulmala, M. Enhancing effect of dimethylamine in sulfuric acid nucleation in the presence of water – a computational study. *Atmos. Chem. Phys.* **2010**, *10*, 4961-4974.
45. Shao, R. J.; Stangeland, A. Amines used in CO_2 capture - health and environmental impacts. Bellona Report, Oslo, Norway, **2009**.
46. Rubin, E. S.; Rao, A. B. A technical, economic, and environmental assessment of amine-based CO_2 technology for power plant greenhouse gas control. *Environ. Sci. Technol.* **2002**, *36* (20), 4467-4475.
47. Stevens, R. G.; Pierce, J. R.; Brock, C. A.; Reed, M. K.; Crawford, J. H.; Holloway, J. S. Ryerson, T. B.; Huey, L. G.; Nowak, J. B. Nucleation and growth of sulfate aerosol in coal-fired power plant plumes: sensitivity to background aerosol and meteorology. *Atmos. Chem. Phys.* **2012**, *12*, 189-206.
48. Adams, P. J.; Seinfeld, J. H. Predicting global aerosol size distributions in general circulation models. *J. Geophys. Res.* **2002**, *107(D19)*, 4370, doi:10.1029/2001JD001010.
49. Pierce, J. R.; Adams, P. J. Uncertainty in global CCN concentrations from uncertain aerosol nucleation and primary emission rates. *Atmos. Chem. Phys.* **2009**, *9*, 1339-1356.
50. Khairoutdinov, M. F.; Randall, D. A. Cloud-resolving modeling of the ARM summer 1997 IOP: Model formulation, results, uncertainties and sensitivities. *J. Atmos. Sci.* **2003**, *60*, 607-625.

51. Merikanto, J.; Napari, I.; Vehkamäki, H.; Anttila, T.; Kulmala, M. New parameterization of sulfuric acid-ammonia-water ternary nucleation rates at tropospheric conditions. *J. Geophys. Res.* **2006**, *112*, D15207, doi:10.1029/2006JD007977.
52. Napari, I.; Noppel, M.; Vehkamäki, H.; Kulmala, M. Parametrization of ternary nucleation rates for H_2SO_4-NH_3-H_2O vapors. *J. Geophys. Res.* **2002**, *107(D19)*, 4381, doi:10.1029/2002JD002132.
53. Westervelt, D. M.; Riipinen, I.; Pierce, J. R.; Trivitayanurak, W.; Adams, P. J. Formation, growth, and cloud condensation nuclei production of nucleated particles: comparison of observations to a global aerosol microphysics model. *Atmos. Chem. Phys.* 2011, in preparation.
54. *Estimating ammonia emissions from stationary power plants.* EPRI, Palo Alto, CA, **2009**, 1017985.

List of figures

Figure 1. Hourly-averaged mixing ratios of NH_3, HNO_3, HCl and CO and concentrations of NH_4^+, SO_4^{2-}, NO_3^- and Cl^- as well as meteorological parameters during the measurements.

Figure 2. Time series of the saturation ratios of NH_4NO_3 and NH_4Cl.

$$S = P_{NH_3} P_{HNO_3} / K_{NH_4NO_3} \; or \; P_{NH_3} P_{HCl} / K_{NH_4Cl}$$

where S is saturation ratio; P is partial pressure; K is dissociation constant.

$K=\exp[84.6-24220/T-6.1\ln(T/298)]$ for NH_4NO_3

$K=\exp[2.2358\ln T-2.13204*10^{4}T^{-1}+65.437516-8.167*10^{-3}T+4.64383*10^{-7}T^{2}$

$-1.10475*10^{-10}T^{3}]$ for NH_4Cl

where T is temperature in Kelvin.

Figure 3. Linear relationship between measured cations and anions.

Figure 4. Time series of gas fractions for NH_3, HNO_3 and HCl.

Figure 5. Time series of the ratio of NH_3 to the sum of HNO_3 and HCl.

Figure 6. The number of particles formed by nucleation in the Parish plume per SO_2 mass emitted as a function of the distance downwind from the Parish plant.

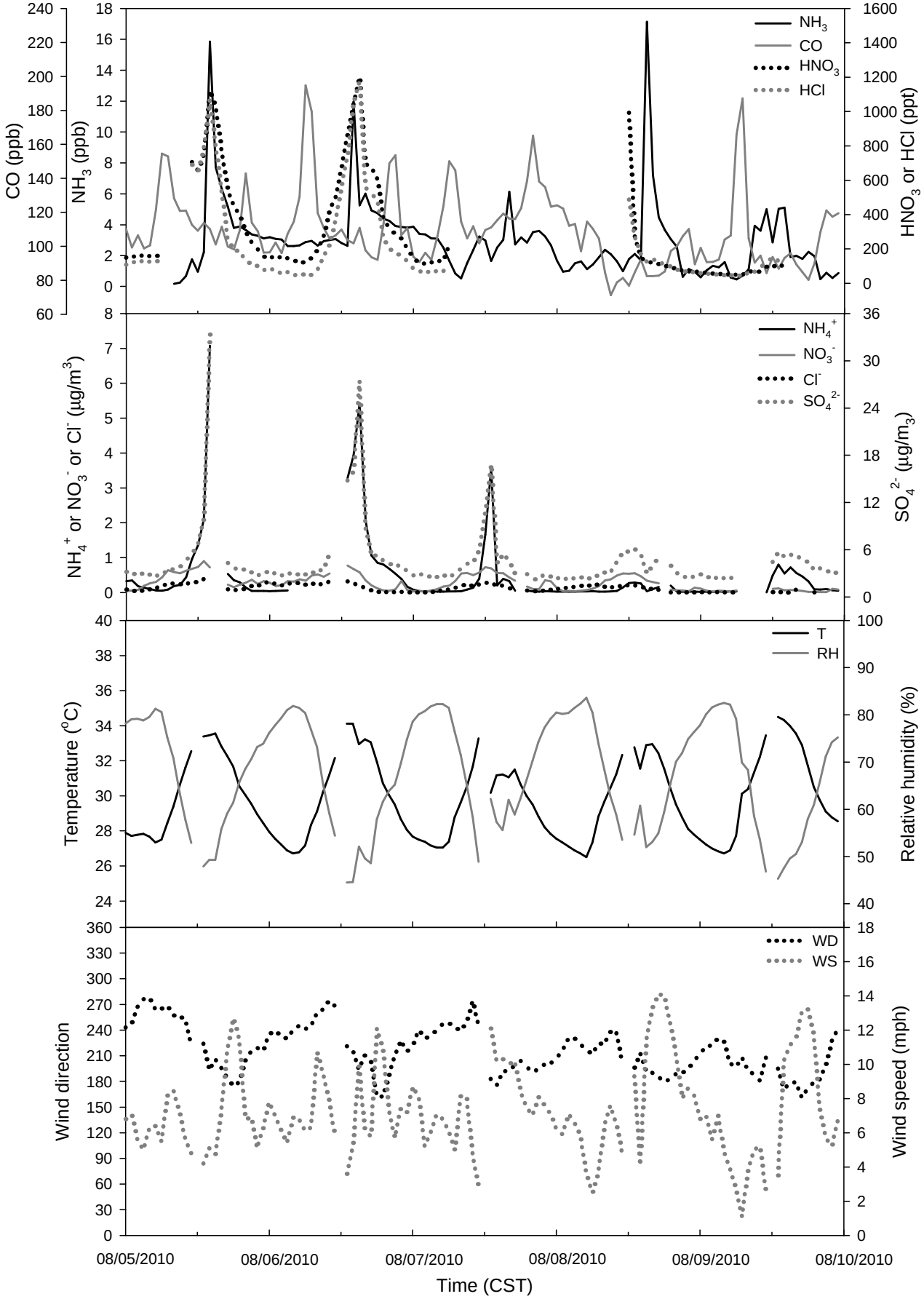
CO (ppb)
NH3 (ppb)
HNO3 or HCl (ppt)
NH3
CO
HNO3
HCl
NH4+ or NO3- or Cl- (μg/m3)
SO4 2- (μg/m3)
NH4+
NO3-
Cl-
SO4 2-
Temperature (°C)
Relative humidity (%)
T
RH
Wind direction
Wind speed (mph)
WD
WS
08/05/2010
08/06/2010
08/07/2010
08/08/2010
08/09/2010
08/10/2010
Time (CST)

Figure 1.

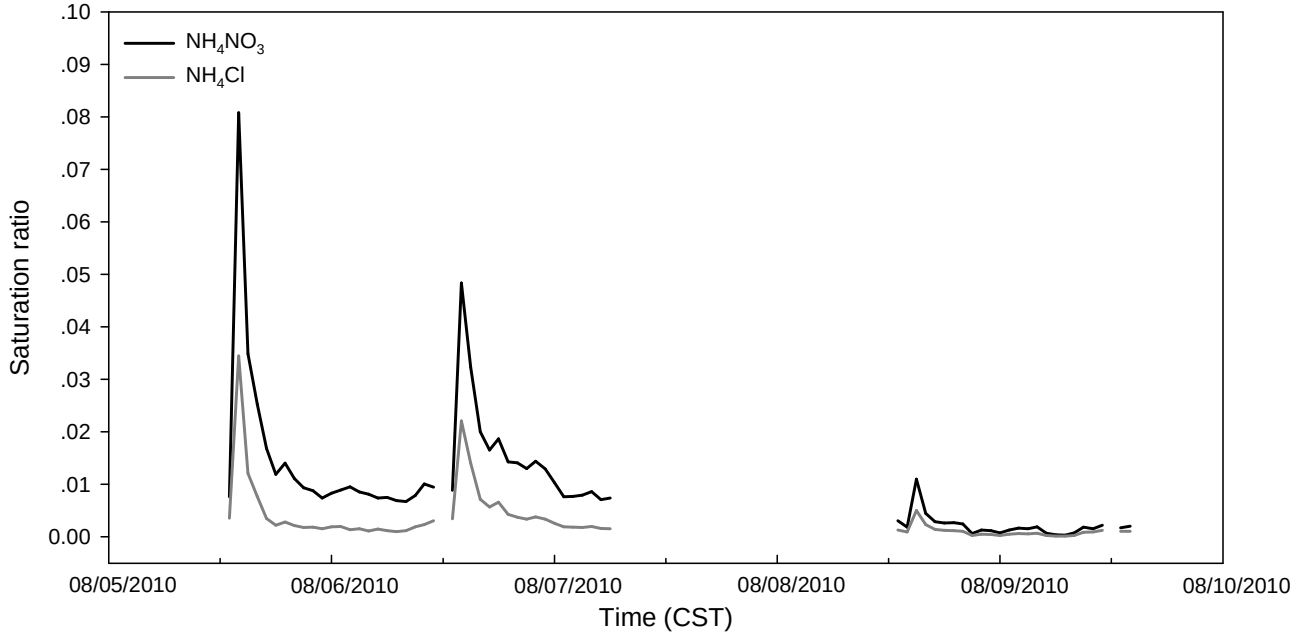
NH_4NO_3
NH_4Cl
Saturation ratio
.10
.09
.08
.07
.06
.05
.04
.03
.02
.01
0.00
08/05/2010
08/06/2010
08/07/2010
08/08/2010
08/09/2010
08/10/2010
Time (CST)

Figure 2.

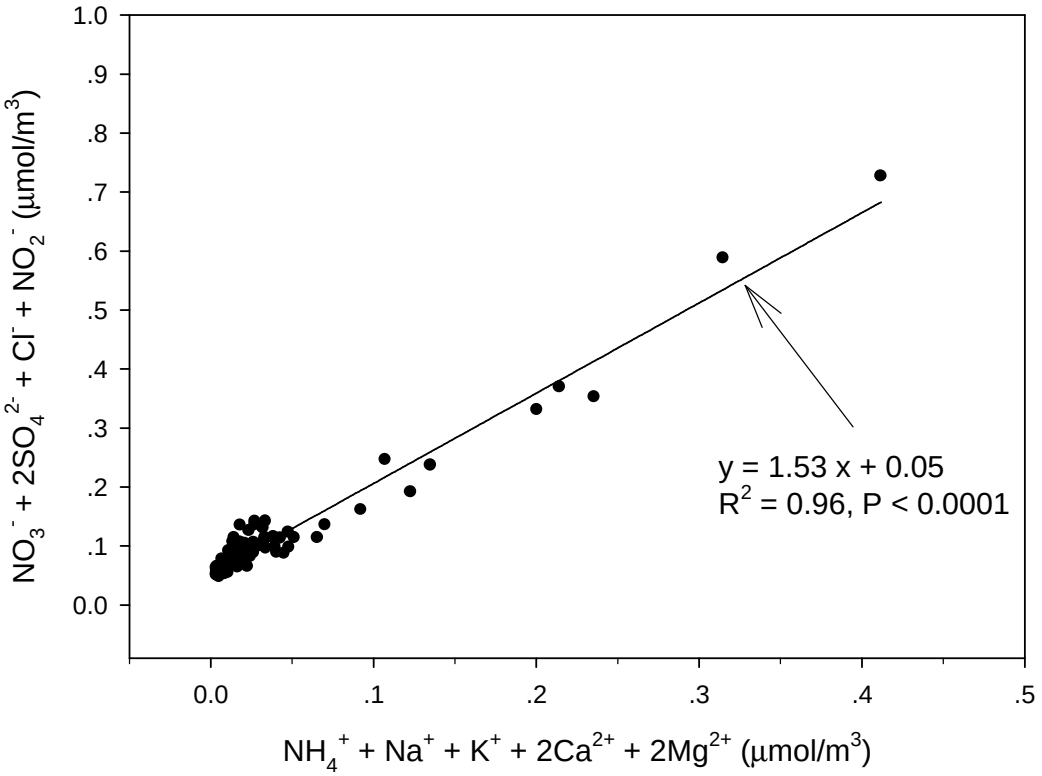
1.0
.9
.8
.7
.6
.5
.4
.3
.2
.1
0.0
0.0
.1
.2
.3
.4
.5
$NO_3^- + 2SO_4^{2-} + Cl^- + NO_2^-$ (µmol/m^3)
$NH_4^+ + Na^+ + K^+ + 2Ca^{2+} + 2Mg^{2+}$ (µmol/m^3)
y = 1.53 x + 0.05
R^2 = 0.96, P < 0.0001

Figure 3.

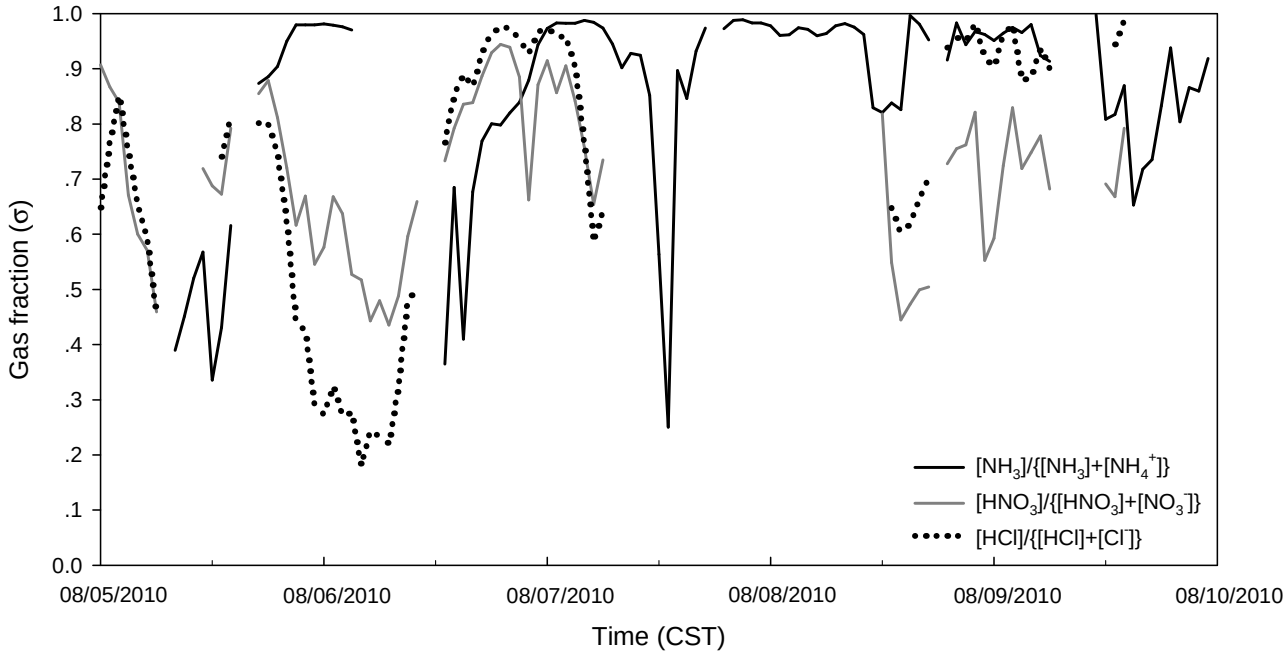
1.0
.9
.8
.7
.6
.5
.4
.3
.2
.1
0.0
Gas fraction (σ)
08/05/2010
08/06/2010
08/07/2010
08/08/2010
08/09/2010
08/10/2010
Time (CST)
[NH3]/{[NH3]+[NH4+]}
[HNO3]/{[HNO3]+[NO3-]}
[HCl]/{[HCl]+[Cl-]}

Figure 4.

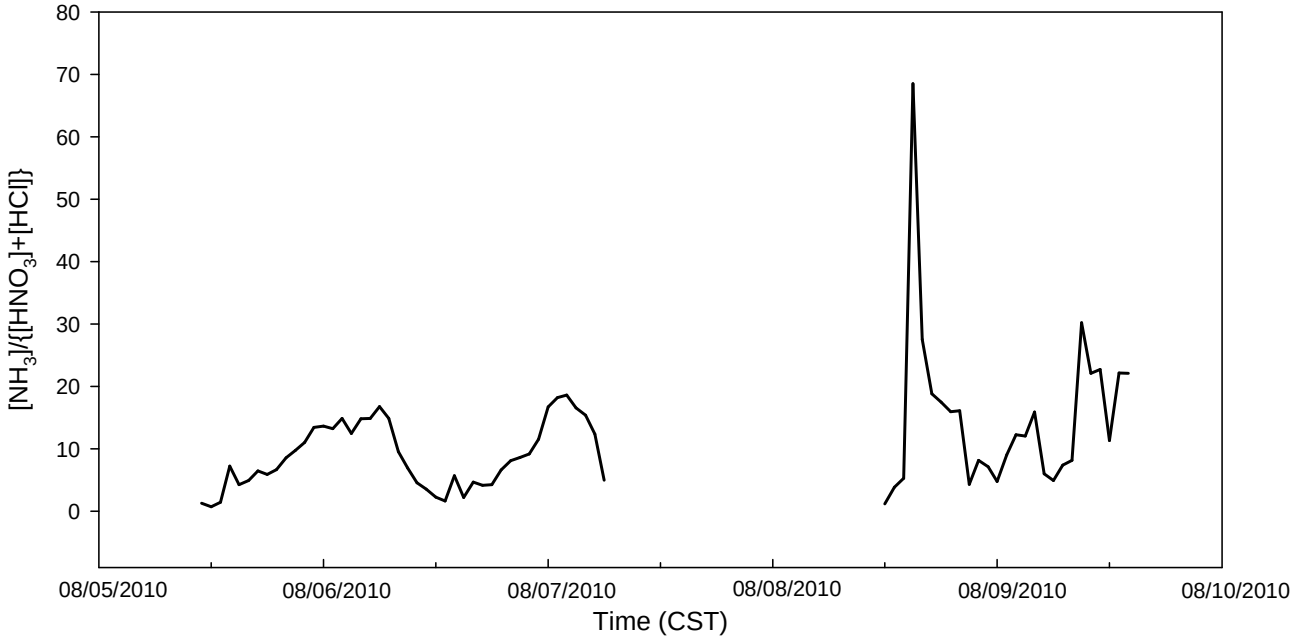
80
70
60
50
40
30
20
10
0
[NH3]/{[HNO3]+[HCl]}
08/05/2010
08/06/2010
08/07/2010
08/08/2010
08/09/2010
08/10/2010
Time (CST)

Figure 5.

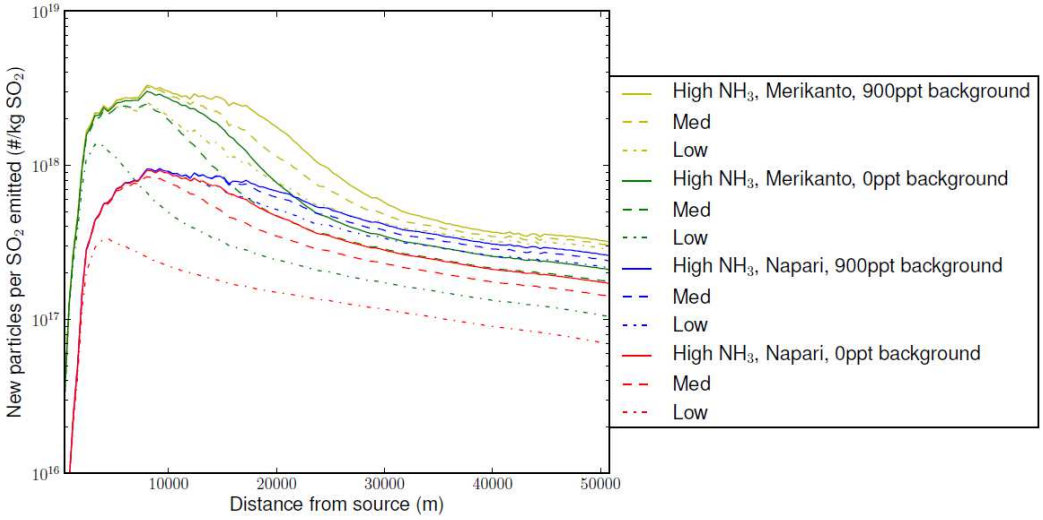
New particles per SO_2 emitted (#/kg SO_2)
10^{19}
10^{18}
10^{17}
10^{16}
10000
20000
30000
40000
50000
Distance from source (m)
High NH_3, Merikanto, 900ppt background
Med
Low
High NH_3, Merikanto, 0ppt background
Med
Low
High NH_3, Napari, 900ppt background
Med
Low
High NH_3, Napari, 0ppt background
Med
Low

Figure 6.

SYNOPSIS TOC